About 2D Cavity Resonance

May 12, 2026

July 26, 2026 Revised

Takuya Yabu(takuya.yabu@live.jp)

Abstract

Research on automobile whistling and suction sounds has been conducted in the past. For cavity resonance, a type of whistling sound, the cavity resonance frequency has been determined using Rossiter's empirical formula. Therefore, we limited our study to the two-dimensional case and clarified the physical phenomena that arise by solving a set of partial differential equations that explain the phenomenon. As a result, the horizontal resonance frequency was found to become proportional to the speed of sound as the mainstream velocity increased, and the resonance frequency of the cavity space was also determined. Finally, we discussed the conditions under which resonance increases. Finally, we were able to confirm the conditions under which resonance increases through numerical calculations.

Nomenclature

L_H: Maximum hole length

ρ, c: Air density and air sound speed

ω: Angular frequency

f_x: Frequency obtained from Rossiter's formula

f_{xr}, f_y: x-direction resonance frequency and y-direction resonance frequency

k: Wavenumber

t: Time

j: Imaginary unit

U, U_{vx}: Mainstream air velocity and vortex (vorticity) velocity

κ: Ratio of vortex (vorticity) velocity to mainstream air velocity

$\hat{G}_v(s)$: Fluid-driven gain

ϕ_v: Phase lag component of the fluid-driven gain

θ_{2D}: Phase lag component caused by the cavity space

M: Mach number

ζ: Vorticity

α: Efficiency of conversion from vorticity to sound pressure (dimension: L^2)

β: Efficiency of conversion from sound pressure to vorticity (dimension: $\mathrm{L}^2\mathrm{M}^{-1}\mathrm{T}^1$)

$\delta(x)$: Dirac delta function

$\delta'(x)$: Differential of Dirac delta function

$H(x)$: Heaviside step function

s: Complex number

L_y: Depth of the box

L_z: Length of the box in the depth direction relative to the direction in the mainstream air velocity

$u(x,y,t), v(x,y,t)$: Velocity in the x direction and velocity in the y direction

1. Introduction

In the past, research has been conducted on the whistling and suction sounds of automobiles (Calvo, Diaz, & San Roman, 2005) (Chien-Hsiung, Lung-Ming , Chang-Hsien , Yen-Loung , & Jik-Chang , 2009) (George, 1990) (Jagtiani, 1972) (Jung & Oh, 1995) (Münder & Carbon, 2022) (Oettle & Sims-Williams, 2017) (Qatu, Abdelhamid, Pang, & Sheng, 2009) (Wang, Chen, & Zhang, 2021) (Zhang, Meng, Li, & Zheng, 2022). Cavity resonance is a type of whistling sound. In cavity resonance, the cavity resonance frequency has traditionally been determined using Rossiter formula, an empirical formula. Therefore, for cavity resonance in the two-dimensional case, we will clarify the physical phenomena that arise by solving the set of partial differential equations that explain the phenomenon. Finally, we will examine the conditions under which resonance increases in numerical calculations.

These will be discussed below.

2. About 2D Cavity Resonance

2.1. Vorticity Movement Equation

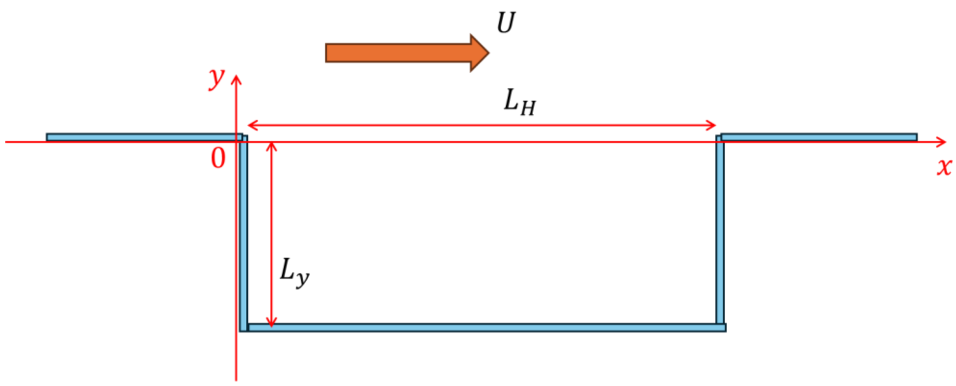

Fig. 1 2-Dimensional Box with Hole

Fig. 1 shows a box with a hole. Here, the conventional definitions of cavity resonance and cavity resonance frequency are given below.

Definition :

When air is flowing at velocity U and there is a hole, a vortex moves from the upstream end to the downstream end of the hole. This vortex collides with the downstream end, generating sound. This generated sound then moves from the downstream end to the upstream end. Sound is a change accompanied by particle velocity, and this particle velocity then collides with the upstream end, generating another vortex. This series of phenomena is defined as "cavity resonance." Furthermore, the reciprocal of the time from when a vortex moves and generates sound until another vortex is generated is defined as the "cavity resonance frequency."

Based on this definition, we derive the differential equation representing cavity resonance, limited to two dimension. First, the movement equation of vorticity $\zeta(x, y, t)$ is expressed by the following equation. However, the viscosity term is ignored.

$$\frac{\partial \zeta}{\partial t} + U_{vx}\frac{\partial \zeta}{\partial x} = 0 \qquad (1)$$

2.2. Powell's Equation

Next, we will find the relationship between sound pressure and vorticity.

Powell's equation is the relationship between sound pressure and vorticity. Expressed in two dimension, Powell's equation is given by the following:

$$\frac{1}{c^2}\frac{\partial^2 p}{\partial t^2} - \left(\frac{\partial^2 p}{\partial x^2} + \frac{\partial^2 p}{\partial y^2}\right)$$
$$= \alpha\rho[\zeta(L_H, 0, t)u(L_H, 0, t)\delta'(x - L_H)\delta(y) - \zeta(L_H, 0, t)v(L_H, 0, t)\delta(x - L_H)\delta'(y)] \qquad (2)$$

2.3. Initial Conditions

The initial condition for the velocity in the x-direction is given below:

$$u(x, y \geq 0, 0) = U \qquad (3)$$

The initial condition for the velocity in the y-direction is given below:

$$v(x, y, 0) = 0 \qquad (4)$$

The initial condition for the sound pressure is given below:

$$p(x, y, 0) = 0 \qquad (5)$$

The initial condition for the time derivative of the sound pressure is given below:

$$\left.\frac{\partial p}{\partial t}\right|_{t=0} = 0 \tag{6}$$

2.4. Boundary Conditions

We need to find the boundary conditions under which the velocity of the returned particles changes to vorticity. These are given by the following equation:

$$\zeta(0,0.t) = -\beta_x \left.\frac{\partial p}{\partial x}\right|_{(x=0,y=0,t=t)} \tag{7}$$

Furthermore, assuming that sound pressure is completely reflected at the bottom of the box and becomes zero at the open end, the following conditions hold true.

$$\left.\frac{\partial p}{\partial x}\right|_{y=-L_y} = 0 \tag{8}$$

Furthermore, assuming that the sound pressure is completely reflected by the left and right walls, the following conditions hold true.

$$\left.\frac{\partial p}{\partial x}\right|_{x=0,-L_y\le y\le 0} = 0 \tag{9}$$

$$\left.\frac{\partial p}{\partial x}\right|_{x=L_H,-L_y\le y\le 0} = 0 \tag{10}$$

3. Resonance Frequency of a Two-Dimensional Cavity Resonance

3.1. Solution to the Vorticity Transfer Equation

We derive the resonance frequency of a two-dimensional cavity resonance. First, we solve equation (1). The solution when the boundary condition is $\zeta(0,t)$ is given by the following equation:

$$\zeta(x,y,t) = \zeta\left(0,0,t - \frac{x}{U_{vx}}\right) \tag{11}$$

3.2. Sound Pressure Equation Using Green's Function Derived from Powell's Equation

Next, we solve Powell's equation (2). This can be obtained using the Green's function in the following form. First, the Green's function is given by the following equation.

$$G(x,y,t|x',y',\tau) = \frac{c}{2\pi}\frac{H(c(t-\tau)-r')}{\sqrt{c^2(t-\tau)^2 - r'^2}} \tag{12}$$

Here, the following equation holds true.

$$r' = \sqrt{(x-x')^2 + (y-y')^2} \tag{13}$$

From equations (2) and (12), the following equation is obtained.

$$p(x,y,t) = -\frac{\alpha\rho c}{2\pi}\sum_{n=-\infty}^{\infty}\int_0^{t-\frac{r_{n,1}}{c}}\frac{\Phi_{n,1}(\tau)}{\sqrt{c^2(t-\tau)^2 - r_{n,1}^2}}d\tau$$

$$+\frac{\alpha\rho c}{2\pi}\sum_{n=-\infty}^{\infty}\int_0^{t-\frac{r_{n,2}}{c}}\frac{\Phi_{n,2}(\tau)}{\sqrt{c^2(t-\tau)^2 - r_{n,2}^2}}d\tau \tag{14}$$

Here, the following equation holds true.

$$\Phi_{n,1}(\tau) = \frac{(u(L_H,0,\tau)\cdot(x-(2n+1)L_H) - (-1)^n\cdot v(L_H,0\,,\tau)\cdot y)\zeta(L_H,0,\tau)}{c^2(t-\tau)^2 - r_{n,1}^2} \tag{15}$$

$$r_{n,1} = \sqrt{(x-(2n+1)L_H)^2 + y^2} \tag{16}$$

$$\Phi_{n,2}(\tau) = \frac{\left(u(L_H,0,\tau)\cdot(x-(2n+1)L_H) - (-1)^n\cdot v(L_H,0\,,\tau)\cdot\left(y+2L_y\right)\right)\zeta(L_H,0,\tau)}{c^2(t-\tau)^2 - r_{n,2}^2} \tag{17}$$

$$r_{n,2} = \sqrt{(x-(2n+1)L_H)^2 + \left(y+2L_y\right)^2} \tag{18}$$

3.3. Stability Condition and Frequency in the Mainstream Air Velocity Direction and Cavity Resonance Frequency

We consider the stability conditions for the solution obtained in Equation (14). Applying the Laplace transform to both sides yields the following equation, where we set $u(L_H,0,s) = U$. To examine stability, we assume $\zeta(L_H,0,s) = \zeta_0 e^{st}$ and $v(L_H,0,s) = v_0 e^{st}$. Additionally, $K_0(x)$ denotes the modified Bessel function of the second kind.

$$p(x,y,s) = -\frac{\alpha\rho c}{2\pi}\sum_{n=-\infty}^{\infty}(U(x-(2n+1)L_H) - (-1)^n v_0 y e^{st})\zeta_0 e^{st}\cdot\frac{1}{c}K_0\left(\frac{r_{n,1}}{c}s\right)$$

$$+\frac{\alpha\rho c}{2\pi}\sum_{n=-\infty}^{\infty}\left(U(x-(2n+1)L_H) - (-1)^n v_0\left(y+2L_y\right)e^{st}\right)\zeta_0 e^{st}\cdot\frac{1}{c}K_0\left(\frac{r_{n,2}}{c}s\right) \tag{19}$$

Here, since linear theory is employed, the term e^{2st} can be neglected as an infinitesimal quantity. Consequently, the following equation is obtained:

$$p(x,y,s) = -\frac{\alpha\rho U\zeta_0}{2\pi}\sum_{n=-\infty}^{\infty}(x-(2n+1)L_H)K_0\left(\frac{r_{n,1}}{c}s\right)e^{st}$$

$$+\frac{\alpha\rho U\zeta_0}{2\pi}\sum_{n=-\infty}^{\infty}(x-(2n+1)L_H)K_0\left(\frac{r_{n,2}}{c}s\right)e^{st} \tag{20}$$

Considering that self-excited oscillations arise when a vortex generated at the upstream edge of the cavity—relative to the mainstream flow—strikes the downstream edge to produce sound, and that sound then travels back from the downstream edge to the upstream edge, the following equation is obtained. Here, we set $p(x,y,s) = p_0 e^{st}$.

$$p_0 e^{st} = -\frac{\alpha\rho U\zeta_0 x}{2\pi} e^{st} e^{-s\left(\frac{L_H}{U_{vx}}+\frac{L_H}{c}\right)} \sum_{n=-\infty}^{\infty} (x-(2n+1)L_H)\left(K_0\left(\frac{r_{n,1}}{c}s\right)-K_0\left(\frac{r_{n,2}}{c}s\right)\right) \tag{21}$$

Therefore, letting $\hat{G}_v(s)$ represent the fluid-driven gain, the characteristic equation is given by the following expression:

$$1-\hat{G}_v(s)\left(-\frac{\alpha\rho U\zeta_0 x}{2\pi}\sum_{n=-\infty}^{\infty}(x-(2n+1)L_H)\left(K_0\left(\frac{r_{n,1}}{c}s\right)-K_0\left(\frac{r_{n,2}}{c}s\right)\right)\right)e^{-s\left(\frac{L_H}{U_{vx}}+\frac{L_H}{c}\right)}=0 \tag{22}$$

Consider the frequency f_x in the mainstream air direction. In this case, the following equation holds based on Equation (23). Here, ϕ_v represents the phase lag component of the fluid-driven gain, and θ_{2D} represents the phase lag component caused by the cavity space.

$$-\phi_v-\theta_{2D}-\omega\left(\frac{L_H}{U_{vx}}+\frac{L_H}{c}\right)=-2\pi n$$

$$2\pi\left(n-\frac{\phi_v+\theta_{2D}}{2\pi}\right)=2\pi f_x\left(\frac{L_H}{U_{vx}}+\frac{L_H}{c}\right)$$

$$f_x=\frac{\left(n_x-\frac{\phi_v+\theta_{2D}}{2\pi}\right)}{\frac{L_H}{U_{vx}}+\frac{L_H}{c}} \tag{23}$$

Finally, by setting $U_{vx}=\kappa U$, the following equation is obtained. Conventionally, a value of 0.25 or close to it has been used for the phase lag in Rossiter's formula. Based on stability conditions, however, it was possible to derive from Equation (22) that $\frac{\phi_v+\theta_{2D}}{2\pi}$ should be used as the phase lag in Rossiter's formula.

$$f_x=\frac{U}{L_H}\frac{\left(n_x-\frac{\phi_v+\theta_{2D}}{2\pi}\right)}{\left(\frac{1}{\kappa}+\frac{U}{c}\right)} \tag{24}$$

Next, applying the Poisson summation formula to the modified Bessel function of the second kind in Equation (22) yields the following equation:

$$1-\hat{G}_v(s)\left(-\frac{\alpha\rho U\zeta_0 x}{2\pi}\sum_{n=-\infty}^{\infty}\left(\frac{e^{-s\frac{|y|}{c}}-e^{-s\frac{|y+2L_y|}{c}}}{s^2+\left(\frac{n\pi c}{L_H}\right)^2}\right)\cos\left(\frac{n\pi c}{L_H}\right)\right)e^{-s\left(\frac{L_H}{U_{vx}}+\frac{L_H}{c}\right)}=0 \tag{25}$$

From this equation, substituting $s=j\omega$ to analyze the stability conditions reveals that the expression diverges to infinity when:

$$\omega=\frac{n\pi c}{L_H} \tag{26}$$

Here, substituting $\omega=2\pi f_{xr}$ and $n=n_{xr}$ yields the following equation:

$$f_{xr} = \frac{n_{xr} c}{2L_H} \tag{27}$$

At this frequency, cavity resonance—a form of self-excited oscillation—occurs. This frequency corresponds to the resonance frequency in the x-direction.

Conversely, based on Equation (25), the resonance frequency in the y-direction given by the following equation does not occur:

$$f_y = \frac{\left(2n_y - 1\right) \cdot c}{4L_y} \tag{28}$$

Unlike the resonance frequency of a standard enclosed space, a frequency f_x in the mainstream air velocity direction is generated first. When this matches the resonance frequency in the x-axis direction, a lock-in phenomenon occurs, resulting in a loud sound.

3.4. Insights from the Frequency in the Mainstream Air Velocity Direction

By further transforming the frequency in the mainstream sir velocity direction (Equation (24)) and taking the limit as $U \to \infty$, the following equation is obtained:

$$f_x = \frac{U}{L_H} \frac{\left(n_x - \frac{\phi}{2\pi}\right)}{\left(\frac{1}{\kappa} + \frac{U}{c}\right)} \to \frac{\left(n_x - \frac{\phi}{2\pi}\right)}{L_H} c \tag{29}$$

In other words, as the mainstream velocity increases, the frequency in the mainstream direction becomes proportional to the speed of sound.

3.5. Sound Pressure at a Position Outside the Sound Source ($x \geq L_H$)

We will now discuss the sound pressure at a position outside the sound source ($x \geq L_H$). As before, it can be calculated using the following equation.

$$p(x, y, t) = \frac{\alpha \rho c}{2\pi} \int_0^{t - \frac{r}{c}} \frac{\left[\frac{1}{c} \frac{\partial}{\partial \tau} \frac{\Phi_{2D}(\tau)}{r} - \frac{1}{r^2} \Phi_{2D}(\tau)\right]}{\sqrt{c^2 (t - \tau)^2 - r^2}} d\tau \tag{30}$$

Here, the following equation holds true.

$$\Phi_{2D}(\tau) = \left(u(L_H, 0, \tau) \cdot (x - L_H) - v(L_H, 0, \tau) \cdot y\right) \zeta(L_H, 0, \tau) \tag{31}$$

$$r = \sqrt{(x - L_H)^2 + y^2} \tag{32}$$

3.6. Incorporating Periodic Boundary Conditions

The discussion thus far has been limited to a two-dimensional plane, without considering three-dimensional extent. However, in practice, there is often a need to use a two-dimensional calculation as a substitute for a three-dimensional one. Therefore, we consider the case where periodic boundary conditions are applied.

When periodic boundary conditions are introduced, Powell's equation takes the following form:

$$\frac{1}{c^2}\frac{\partial^2 p}{\partial t^2}+\frac{2\gamma}{c}\frac{\partial p}{\partial t}-\left(\frac{\partial^2 p}{\partial x^2}+\frac{\partial^2 p}{\partial y^2}\right)$$
$$=\alpha\rho[\zeta(L_H,0,t)u(L_H,0,t)\delta'(x-L_H)\delta(y)-\zeta(L_H,0,t)v(L_H,0,t)\delta(x-L_H)\delta'(y)] \qquad (33)$$

Here, γ is given by the following equation. L_z represents the dimension of the cavity in the depth direction relative to the main flow direction. It is assumed that no reflection occurs at L_z and that energy escapes.

$$\gamma=\frac{1}{2L_z} \qquad (34)$$

The initial and boundary conditions are the same as those described in Sections 2.3 and 2.4, respectively.

The Green's function for this version of Powell's equation is given by the following expression:

$$G(x,y,t|x',y',\tau)=\frac{c}{2\pi}\frac{H(c(t-\tau)-r')}{\sqrt{c^2(t-\tau)^2-r'^2}}e^{\gamma c(t-\tau)} \qquad (35)$$

Based on the above, the solution for the internal sound pressure when periodic boundary conditions are applied is as follows:

$$p(x,y,t)=-\frac{\alpha\rho c}{2\pi}\sum_{n=-\infty}^{\infty}\int_0^{t-\frac{r_{n,1}}{c}}\frac{\Phi_{n,1}(\tau)\cdot e^{\gamma c(t-\tau)}}{\sqrt{c^2(t-\tau)^2-r_{n,1}^2}}d\tau$$
$$+\frac{\alpha\rho c}{2\pi}\sum_{n=-\infty}^{\infty}\int_0^{t-\frac{r_{n,2}}{c}}\frac{\Phi_{n,2}(\tau)\cdot e^{\gamma c(t-\tau)}}{\sqrt{c^2(t-\tau)^2-r_{n,2}^2}}d\tau \qquad (36)$$

The symbols are the same as those in Section 3.2. The conclusions regarding the stability condition, the frequency in the mainstream direction, and the cavity resonance frequency are the same as those in Section 3.3.

The solution for the external sound pressure when periodic boundary conditions are applied is given by the following equation:

$$p(x,y,t)=\frac{\alpha\rho c}{2\pi}\int_0^{t-\frac{r}{c}}\frac{\left[\frac{1}{c}\frac{\partial}{\partial\tau}\frac{\Phi_{2D}(\tau)\cdot e^{\gamma c(t-\tau)}}{r}-\frac{1}{r^2}\Phi_{2D}(\tau)\cdot e^{\gamma c(t-\tau)}\right]}{\sqrt{c^2(t-\tau)^2-r^2}}d\tau \qquad (37)$$

The symbols are the same as those in Section 3.5.

4. Numerical Calculations

The results were confirmed by numerical calculation. The values used are shown in Table 1 below.

Furthermore, for $\frac{\partial p}{\partial x}$ and $v(L_H, 0, t)$, it was assumed that vortices were continuously generated at the upstream end at a Rossiter formula primary frequency of 9.6 (Hz), and that this vortex mass was continuously excited at the downstream end as $v(L_H, 0, t)$ at the same Rossiter formula primary frequency of 9.6 (Hz). Therefore, the following equation is continuously used during the numerical calculation. Here, $f_{x,1}$ is the Rossiter formula primary frequency of 9.6 (Hz).

$$\frac{\partial p}{\partial x} = \sin\left(2\pi f_{x,1} t\right) \tag{38}$$

$$v(L_H, 0\,, t) = \frac{1}{2}\sin\left(2\pi f_{x,1} t\right) \tag{39}$$

Table 1 Parameter and Value

Parameter	Value
ρ	1.225(kg/m^3)
c	340.0(m/s)
U	34.0(m/s)
κ	0.6
α	1(m^2)
β_x	0.01(m^{2}s/kg)
$\phi_v + \theta_{2D}$	$\frac{\pi}{2}$
L_H	1.5(m)
L_y	0.7(m)
L_z	1.3(m)

The numerical calculation results are shown in Fig. 2. The observation point was set near the origin at $(x, y) = (0.01, 0.01)$. The upper plot shows the time-series waveform of the sound pressure, while the lower plot shows its frequency characteristics. Case (1) represents the scenario without periodic boundary conditions, and case (2) represents the scenario with periodic boundary conditions.

Observing the time-series waveform in (1) of Fig. 2, one can see a combination of waveforms originating from various sound sources; this is also evident from the frequency characteristics. This occurs because the energy associated with the fundamental frequency peak of Rossiter's equation f_x (9.6 (Hz)) is confined within the two-dimensional plane, causing energy to flow into the resonance frequency f_{xr} (113.3 (Hz)) and its integer multiples. Conversely, for f_y, no oscillation is excited, even though the frequency is close to the resonance frequency of f_x. This supports the discussion regarding Equation (25). Furthermore, the time-series waveform in (1) is increasing. This is because the energy is confined within the plane.

Next, consider (2) of Fig. 2. No peak appears at the resonance frequency f_{xr}. This is because the periodic boundary conditions cause energy to diffuse, preventing it from flowing into the resonance frequency f_{xr}. Furthermore, because energy diffuses due to the periodic boundary conditions, the sound is produced with a constant amplitude.

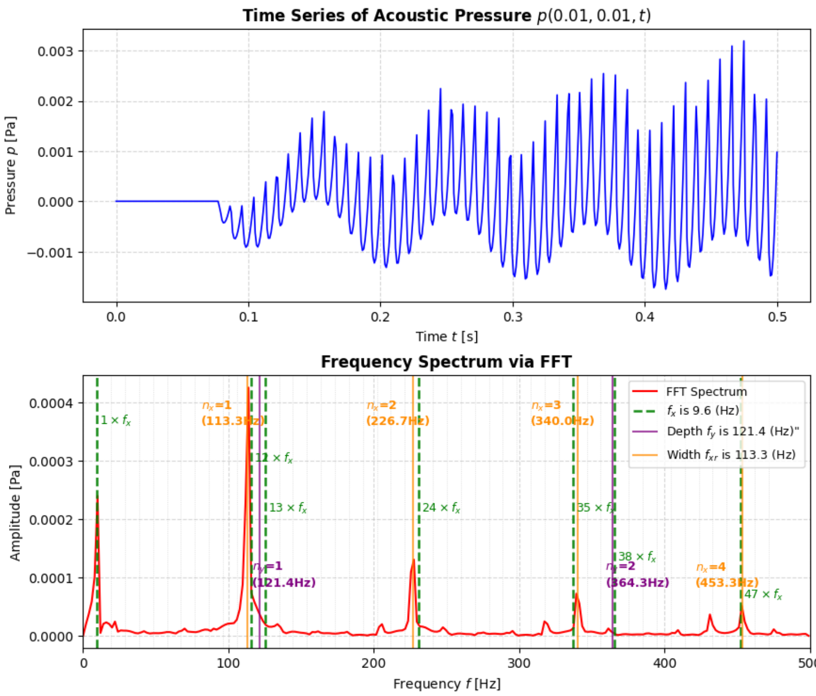

(1)If periodic boundary conditions are not considered

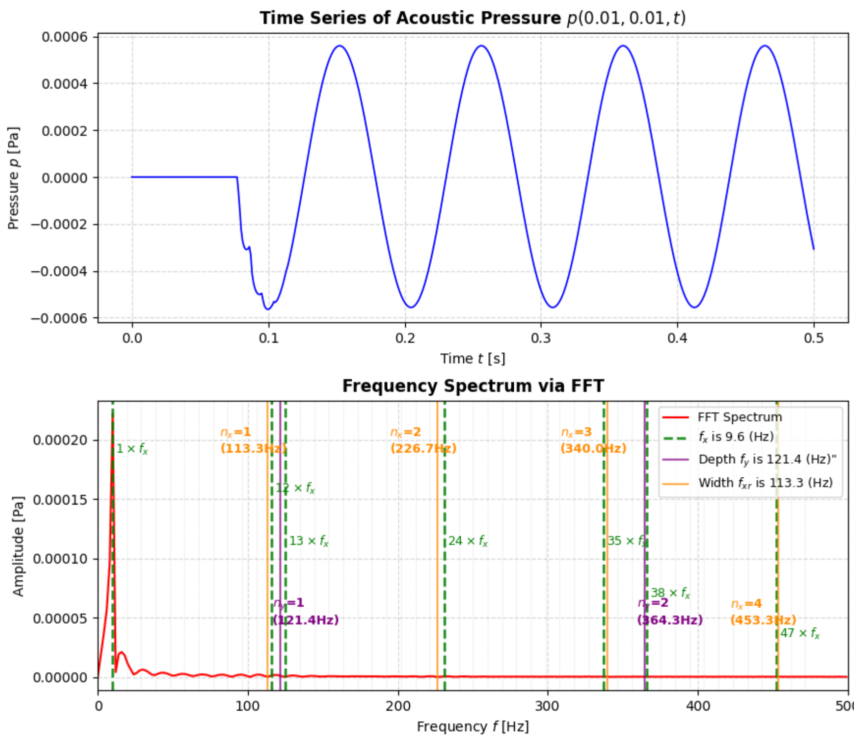

(2)If periodic boundary conditions are considered

Fig. 2 Numerical Calculation Results

Next, we calculate the sound pressure for $x \geq L_H$. The results are shown in Fig. 3. The observation position was $(x, y) = (2.0, 0.5)$. The top graph shows the time-series waveform of the sound pressure, and the bottom graph shows the frequency response of the sound pressure.

From (1) and (2) in Fig. 3, it is evident that time is required for the sound to travel from the source. Furthermore, the frequency characteristics below show a peak at 9.6 (Hz), corresponding to the first-order frequency of Rossiter's formula f_x. This indicates that for $x \geq L_H$, the sound consists solely of frequency components corresponding to the first-order frequency of Rossiter's formula (f_x), which represents the forced oscillation. Additionally, the amplitude in (2) is smaller than that in (1). This difference arises because, in case (1), energy is confined within the plane with no means of escape, leading to increased sound pressure, whereas in case (2), the periodic boundary conditions allow the energy to disperse, resulting in lower sound pressure.

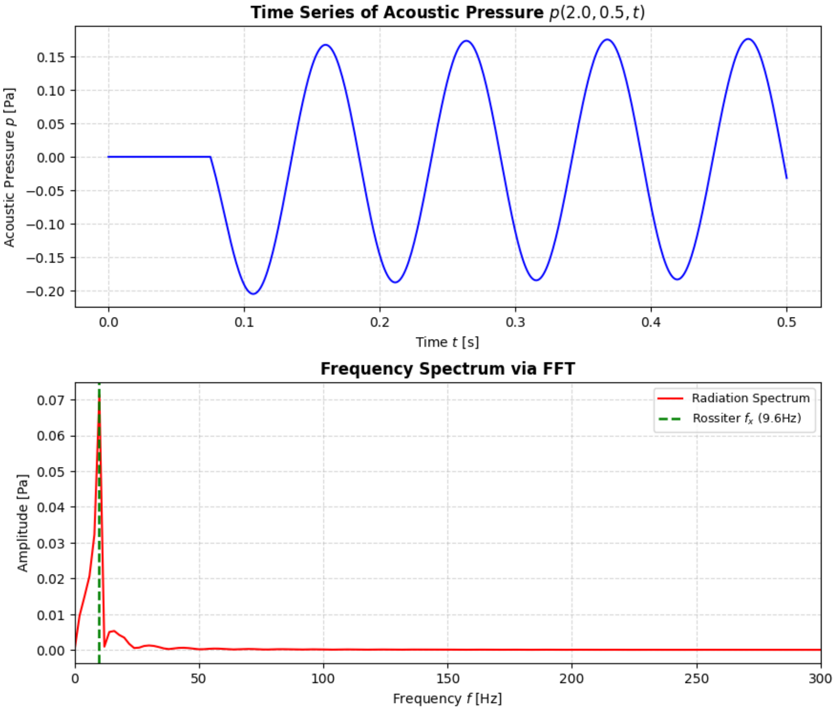

(1) If periodic boundary conditions are not considered

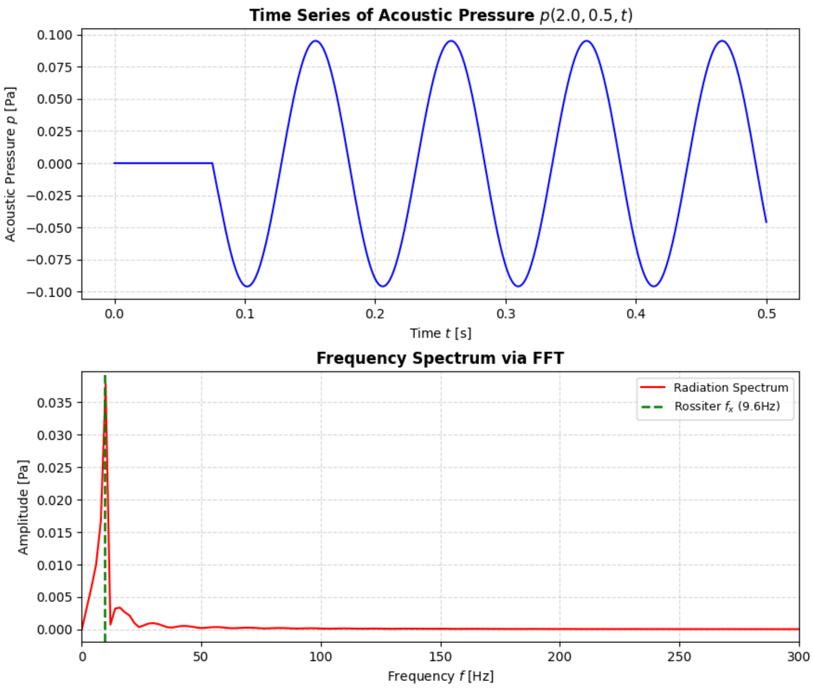

(2)If periodic boundary conditions are considered

Fig. 3 Numerical Calculation Result ($(x, y) = (2.0, 0.5)$)

Next, Fig. 4 shows the numerical calculation results for $U = 1133.3$ (m/s), with the observation point set near the origin at $(x, y) = (0.01, 0.01)$. Case (1) represents the scenario without periodic boundary conditions, while case (2) represents the scenario with periodic boundary conditions.

In both (1) and (2), the fundamental frequency of f_x matches the fundamental resonant frequency of f_{xr}, and it can be seen that a very loud sound is being generated. Furthermore, in both cases (1) and (2), a peak appears only at the first resonance frequency of f_{xr}, indicating the occurrence of a lock-in phenomenon. However, the sound pressure increases in case (1), whereas it remains nearly constant in case (2). This difference arises because, in case (1), energy is confined within the plane with no escape route, causing the sound pressure to rise, while in case (2), the periodic boundary conditions allow energy to dissipate, resulting in a nearly constant sound pressure.

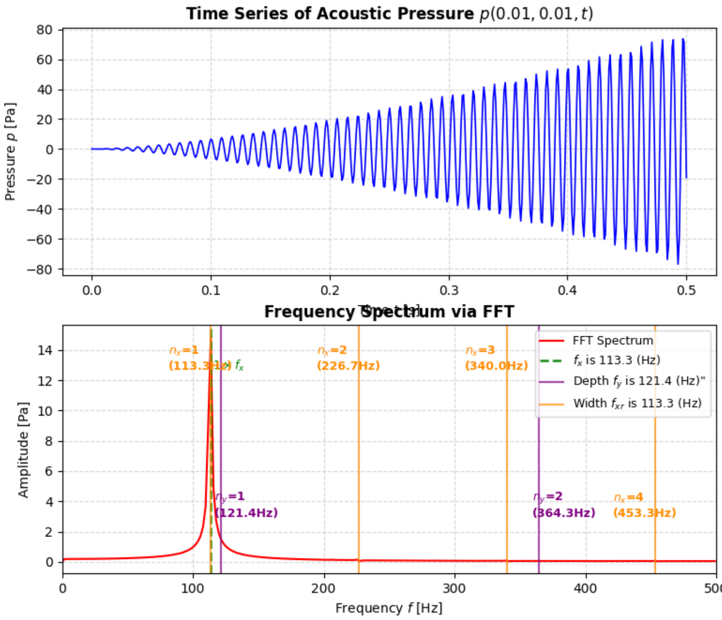

(1)If periodic boundary conditions are not considered

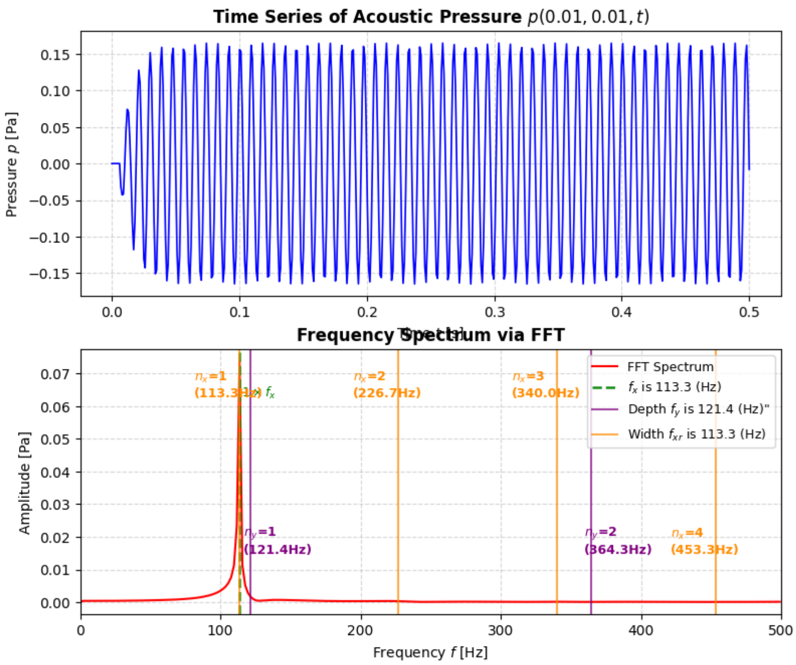

(2)If periodic boundary conditions are considered

Fig. 4 Numerical Calculation Result (U = 1133.3(m/s))

Next, Fig. 5 shows the numerical calculation results for $U = 1700.0$ (m/s), with the observation point set at $(x, y) = (0.01, 0.01)$ near the origin. Case (1) represents the scenario without periodic boundary conditions, while Case (2) represents the scenario with periodic boundary conditions.

In (1), it can be seen that the first-order frequency of f_x and the first-order resonance frequency of f_{xr} are excited; in fact, the peak at the first-order resonance frequency of f_{xr} is even larger. Furthermore, the first- and second-order resonance frequencies of f_y are not excited. Additionally, regarding resonance in the x-direction, small peaks appear at the second- and third-order resonance frequencies, a result that corroborates the discussion concerning Equation (25). Conversely, in (2), there are no peaks at the resonance frequencies in the x-direction. This is because the periodic boundary conditions cause energy to diffuse, preventing it from flowing into the resonance frequencies of f_{xr}. Moreover, while the sound pressure increases in (1), it remains nearly constant in (2). This difference arises because, in (1), energy is confined within the plane with no escape route, leading to an increase in sound pressure, whereas in (2), the periodic boundary conditions allow energy to diffuse, resulting in a nearly constant sound pressure.

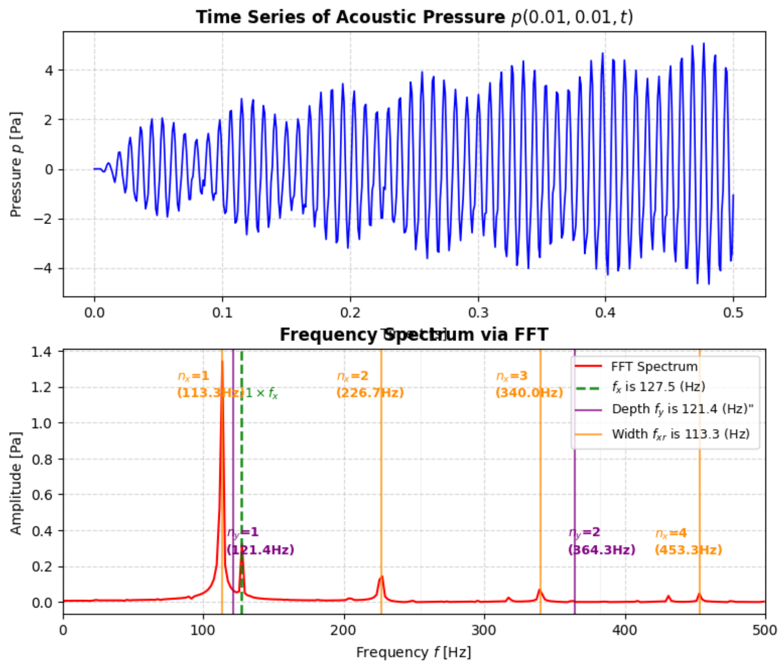

(1) If periodic boundary conditions are not considered

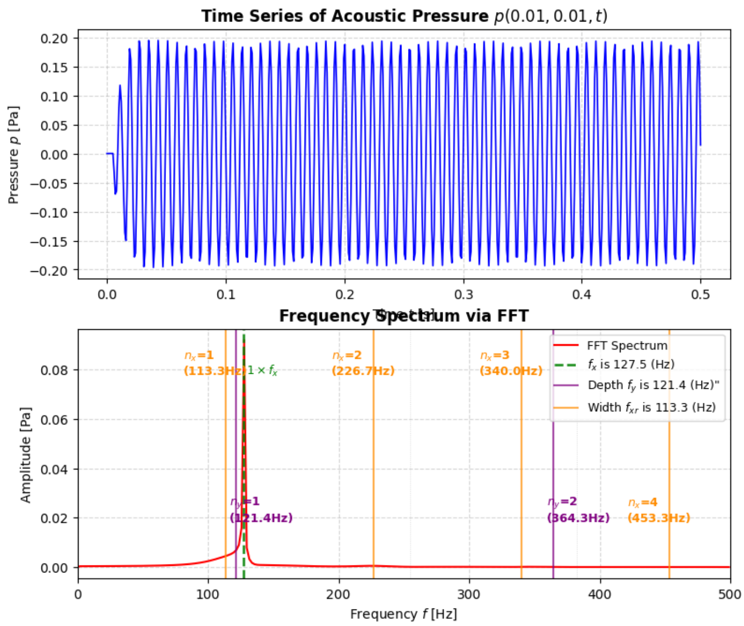

(2)If periodic boundary conditions are considered

Fig. 5 Numerical Calculation Result (U = 1700.0(m/s))

Finally, Fig. 6 shows the numerical calculation results for $U = 1415.5$ (m/s), with the observation point set near the origin at $(x, y) = (0.01, 0.01)$. Case (1) represents the scenario without periodic boundary conditions, while case (2) represents the scenario with periodic boundary conditions.

In (1) and (2), it can be seen that the fundamental frequency of f_x and the fundamental resonance frequency of f_y are present. However, no peak appears at the second resonance frequency of f_y. This suggests that resonance in the y-direction is not being excited; rather, the sound at f_x is being produced. This supports the discussion regarding Equation (25). Furthermore, in (1), small peaks are present at the first, second, and third resonance frequencies associated with x-direction resonance. Notably, the peak at the fundamental resonance frequency of f_x is the largest overall. This also corroborates the discussion concerning Equation (25). Conversely, in (2), there are no peaks at the x-direction resonance frequencies. This is because the periodic boundary conditions cause energy to diffuse, preventing it from concentrating at the resonance frequencies of f_{xr}. Additionally, while the sound pressure increases in (1), it remains nearly constant in (2). This difference arises because, in (1), energy is confined within the plane with no escape route, leading to an increase in sound pressure, whereas in (2), the periodic boundary conditions allow energy to diffuse, resulting in constant sound pressure.

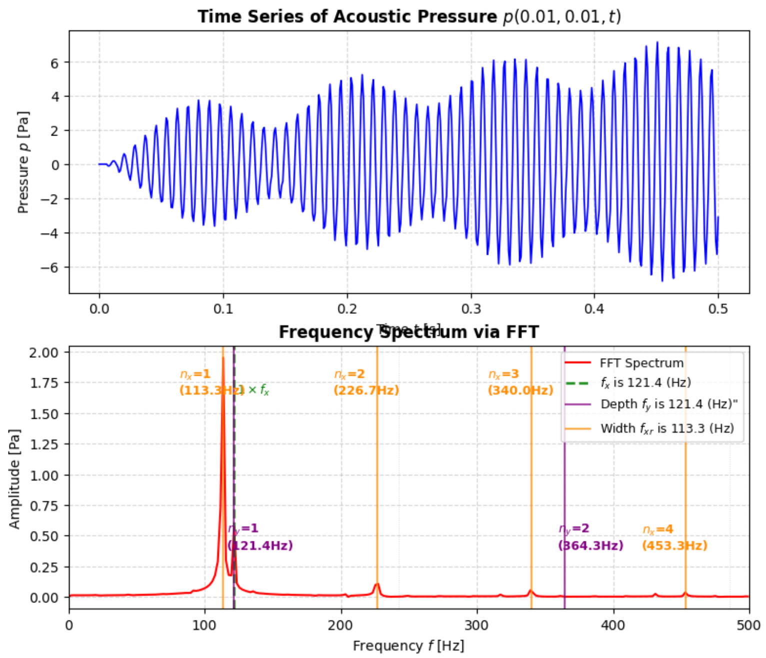

(1) If periodic boundary conditions are not considered

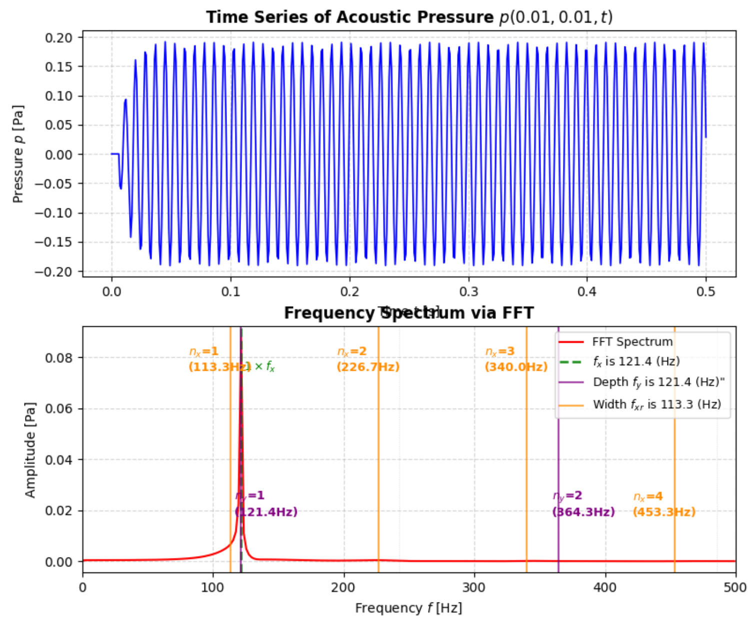

(2)If periodic boundary conditions are considered

Fig. 6 Numerical Calculation Result (U = 1415.5(m/s))

5. Conclusion

Research on automobile whistling and suction sounds has been conducted in the past. For cavity resonance, a type of whistling sound, the cavity resonance frequency has been determined using Rossiter's empirical formula. Therefore, we limited our study to the two-dimensional case and clarified the physical phenomena that arise by solving a set of partial differential equations that explain the phenomenon. As a result, the horizontal resonance frequency was found to become proportional to the speed of sound as the mainstream velocity increased, and the resonance frequency of the cavity space was also determined. Finally, we discussed the conditions under which resonance increases. Finally, we were able to confirm the conditions under which resonance increases through numerical calculations.

References

Calvo, J. A., Diaz, V., & San Roman, J. L. (2005). *Controlling the turbocharger whistling noise in diesel engines.* International Journal of Vehicle Noise and Vibration, Vol. 2, No. 1. doi:https://doi.org/10.1504/IJVNV.2006.008524

Chien-Hsiung, T., Lung-Ming , F., Chang-Hsien , T., Yen-Loung , H., & Jik-Chang , L. (2009). *Computational aero-acoustic analysis of a passenger car with a rear spoiler.* Applied Mathematical Modelling, Volume 33, Issue 9. doi:https://doi.org/10.1016/j.apm.2008.12.004

George, A. R. (1990). *Automobile Aerodynamic Noise.* SAE Transactions, Vol. 99, Section 6. Retrieved from http://www.jstor.org/stable/44553993

Jagtiani, H. (1972). *The Objective Method of Evaluating Aspiration Wind Noise.* SAE Technical Paper 720506. doi:https://doi.org/10.4271/720506

Jung, W., & Oh, S. (1995). *The Influence of Vehicle Elements to Aspiration Wind Noise.* SAE Technical Paper 950624. doi:https://doi.org/10.4271/950624

Münder, M., & Carbon, C.-C. (2022). *Howl, whirr, and whistle: The perception of electric powertrain noise and its importance for perceived quality in electrified vehicles.* Applied Acoustics, Volume 185. doi:https://doi.org/10.1016/j.apacoust.2021.108412

Oettle, N., & Sims-Williams, D. (2017). *Automotive aeroacoustics: An overview.* Journal of Automobile Engineering, Volume 231, Issue 9. doi:https://doi.org/10.1177/0954407017695147

Qatu, M. S., Abdelhamid, M. K., Pang, J., & Sheng, G. (2009). *Overview of automotive noise and vibration.* International Journal of Vehicle Noise and Vibration, Vol. 5, No. 1-2. doi:https://doi.org/10.1504/IJVNV.2009.029187

Wang, Q., Chen, X., & Zhang, Y. (2021). *An Overview of Automotive Wind Noise and Buffeting Active Control.* SAE International Journal of Vehicle Dynamics, Stability, and NVH, 5(4). doi:https://doi.org/10.4271/10-05-04-0030

Zhang, F., Meng, W., Li, X., & Zheng, C. (2022). *A vehicle whistle database for evaluation of outdoor acoustic source localization and tracking using an intermediate-sized microphone array.* Applied Acoustics, Volume 201. doi:https://doi.org/10.1016/j.apacoust.2022.109113